Chemical Interactions at Metal/Molecule Interfaces in Molecular JunctionsA Pathway Towards Molecular Recognition

By *Mila Manolova, Hans-Gerd Boyen,* Jan Kucera, Axel Groß, Andriy Romanyuk, Peter Oelhafen, Valentina Ivanova,* and *Dieter M. Kolb*

Small organic molecules as potential building-blocks for future nanoelectronic devices[1–5] will require new types of sensors able to identify/quantify molecules in appropriate solutions on a single-molecule level. Recently, an elegant new method has been proposed[6] that allows detection of small aromatic units like 4-aminothiophenol (4-ATP) molecules by measuring the tunneling resistance between two metal electrodes separated by a short distance (a few nanometers). While, from a simple point of view, an *increase* in conductivity should be expected because of the bridging of the tunnelling gap by one or more molecules (thus offering molecular orbitals as additional transport channels), a *decreased* conductivity was observed experimentally with a reduction factor that depended on the type of molecule present in the solution. Here, we report on combined experimental and theoretical efforts aimed at unravelling this phenomenon by studying the electronic properties of one of the metal electrodes in such a molecular junction.

For this purpose, a 4-ATP self-assembled monolayer (SAM) has been prepared on top of a Au(111) crystal, which, in a second step, has been metallized by a nearly closed Pd overlayer of monoatomic height by means of a recently developed electrochemical approach.[7–10] Photoelectron spectroscopy together with density functional theory (DFT) taking into account *all contributing parts* of the molecular junction finally allowed analysis of its structural setup and its electronic properties. Angle-resolved X-ray photoelectron spectroscopy (XPS) reveals that the 4-ATP SAM actually consists of a minimum of two molecular layers. Most importantly, using ultraviolet photoelectron spectroscopy (UPS) and DFT simulations, strong chemical interactions between the metal overlayer and the amino groups are found to play a decisive role in determining the overall electronic properties, and thus the transport properties of the SAM/metal contact, as will be demonstrated in the following.

It is well-known that 4-ATP has a strong tendency to form multilayers on Au(111), which lead to scanning tunnelling microscopy (STM) images with considerable height variations and of blurred contrast when it comes to molecular-scale resolution.[11] Even for highly diluted solutions (sub-millimolar concentrations of the 4-ATP), more than just one layer is generally formed. On the other hand, reductive desorption of thiols from gold surfaces is known to occur at electrode potentials negative of −0.1 V vs. standard calomel electrode (SCE), which may be considered an appropriate means for desolving any thiol in excess of the first layer.[12] In Figure 1 cyclic voltammograms are shown for Au(111) in 0.1 M H_2SO_4, after the electrode had been immersed for 15 min in a 0.1×10^{-3} M 4-ATP/0.1 M H_2SO_4 modification solution. While the first cycle (dash-dotted line, start at +0.2 V vs. SCE in the negative direction) was restricted to the stability range of the 4-ATP adlayer, i.e., 0 and +0.4 V, the second cycle (solid line) was extended to much more negative potentials to explore partial reductive desorption. The latter process is clearly reflected in a cathodic current that peaks at −0.18 V. The third cycle (dotted line) now shows double-layer charging behaviour up

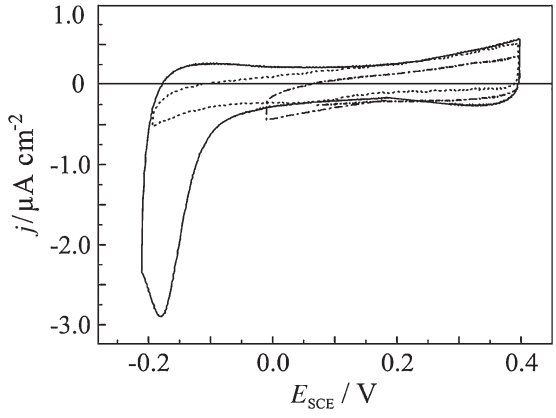

Figure 1. Cyclic voltammograms for a Au(111) electrode in 0.1 M H_2SO_4 that had been immersed in a 0.1×10^{-3} M 4-ATP/0.1 M H_2SO_4 solution for 15 min: first cycle within the stability range of the 4-ATP SAM (dash-dotted line); second cycle with partial reductive desorption of the SAM (solid line); third cycle aquired with a scan rate of 10 mV s^{-1} (dotted line). Scan rate: 5 mV s^{-1}.

[*] Prof. H.-G. Boyen
Institute for Materials Research (IMO)
Hasselt University, 3590 Diepenbeek (Belgium)
E-mail: hansgerd.boyen@uhasselt.be
Dr. M. Manolova, Dr. V. Ivanova,[+] Prof. D. M. Kolb
Institut für Elektrochemie
Universität Ulm, 89069 Ulm (Germany)
Dr. J. Kucera, Prof. A. Groß
Institut für Theoretische Chemie
Universität Ulm, 89069 Ulm (Germany)
Dr. A. Romanyuk, Prof. P. Oelhafen
Institut für Physik
Universität Basel, 4056 Basel (Switzerland)
[+] Present address: LETI/D2NT/LBE, CEA-Grenoble
38054 Grenoble Cedex 9 (France)

DOI: 10.1002/adma.200801634

to −0.2 V, which indicates that a new, more stable situation has been reached. The 4-ATP adlayer structure change concomitant with the second cycle is demonstrated in Figure 2 by in situ STM. In Figure 2a, an image is presented that is typical for an adlayer immediately after modification in 0.1×10^{-3} M 4-ATP/0.1 M H_2SO_4: the first uniform adlayer is covered by islands of a second layer, which gives a rough appearance to the surface. Figure 2b has been recorded after applying a potential cycle down to −0.2 V vs. SCE at a rate of 10 mV s^{-1}, which involves reductive desorption. Indeed, the 4-ATP islands have all disappeared, leaving a uniform adlayer with only a few monoatomic height gold islands on the flat terraces, which are a result of lifting of the reconstructed Au(111) upon contact of the freshly flame-annealed electrode with the modification solution. It is worth mentioning that indications of long-range structural order of the molecules are completely absent for the flat 4-ATP adlayer.

For Pd deposition onto the 4-ATP adlayer, a recently developed procedure[7–10] was followed, which involves immersion of the 4-ATP-modified Au(111) in a 0.1×10^{-3} M solution of $PdSO_4$ to allow complexation between Pd^{2+} ions and the amino group, with subsequent transfer to an electrochemical cell for Pd^{2+} ion reduction in neat 0.1 M H_2SO_4. In situ STM has also been employed to characterize the structure of the electrodeposited Pd on the 4-ATP adlayer, as shown in Figure 2c. Like in former studies on Pd overlayers on top of 4-mercaptopyridine SAMs,[7,8,13,14] monoatomic height islands are seen in line-scans (not shown here), which finally can be assigned to Pd islands *on top* of the 4-ATP adlayer (see below). However, unlike in former studies where the maximum coverage for one single complexation step was about 30%, we now observe a coverage twice as large, namely 60% of a full monolayer. As was demonstrated[7–10] with various metal overlayer systems (Pd, Pt, Rh) on top of 4-mercaptopyridine SAMs, one functional group can usually bind one metal ion. Because a SAM typically consists of about 1/3 of a monolayer of organic molecules (which forms, e.g., a $(\sqrt{3} \times \sqrt{3})$ R30° structure)[15] the total amount of metal deposited with one preparation cycle is expected to be about 1/3 of a monolayer. A coverage of 60% for Pd on 4-ATP, achieved with one complexation cycle, must imply that each functional (amino) group binds two Pd^{2+} ions. Figure 2d finally shows an in situ STM image after immersing a sample that corresponds to Figure 2c into the $PdSO_4$ complexation solution for a second time. Such a procedure was applied in the past to increase the coverage of the electrodeposited metal. Indeed, the Pd coverage could be increased to practically a full monolayer, although a second Pd layer had already started to grow (see inset), which is most likely a result of Pd^{2+} ion adsorption onto the already existing metal islands.

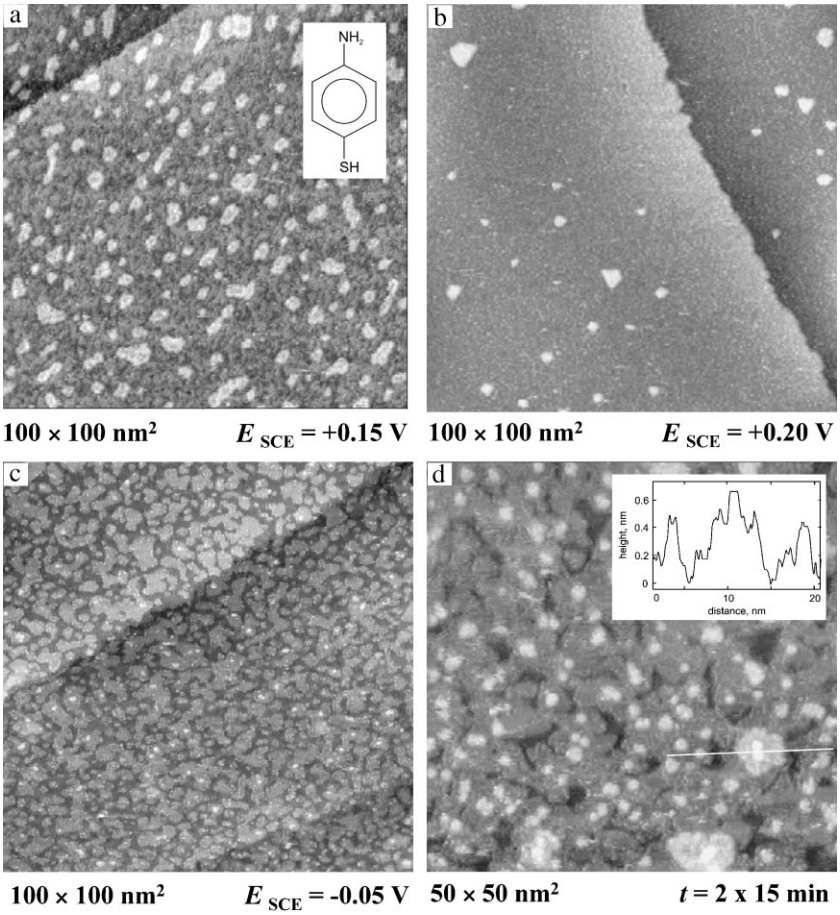

Figure 2. STM images of a 4-ATP-modified Au(111) electrode in 0.1 M H_2SO_4 at indicated potentials before (a) and after (b) partial reductive desorption of the 4-ATP overlayer; The bottom row presents STM images of 4-ATP-modified Au(111) in 0.1 M H_2SO_4 at −0.05 V vs. SCE, after the electrode was immersed in 0.1×10^{-3} M 4-ATP/0.1 M H_2SO_4 for 15 min (c) and after two subsequent complexation cycles (d).

In order to extract more details about the layer sequence of metallized SAMs, angle-resolved XPS has proven to be a versatile tool in the past.[7,9,16] In our case, to avoid complications induced by contributions that arise from the starting growth of a second Pd layer as shown in Figure 2d, a sample corresponding to Figure 2c was chosen for further investigations. Photoemission spectra of element-specific core levels that represent the materials involved (Au $4d_{3/2}$, Au 4f, C 1s, Pd $3d_{3/2}$) were acquired as a function of the detection (emission) angle α, thereby allowing systematic variation of the surface sensitivity of the experiment. An example is given in Figure 3a, where a series of core-level spectra are presented that cover the binding energy range of the Au $4d_{3/2}$ as well as Pd $3d_{3/2}$ core lines. Obviously, by increasing α, the spectroscopic contribution of the Pd $3d_{3/2}$ line is found to systematically grow, thus providing evidence that the Pd layer resides on top rather then underneath the SAM. A more detailed picture emerges from the angular dependence of the integrated core-line intensities: while going from normal incidence ($\alpha = 0°$) to nearly grazing incidence ($\alpha = 80°$), the attenuation of the photoelectrons emitted

ADVANCED MATERIALS

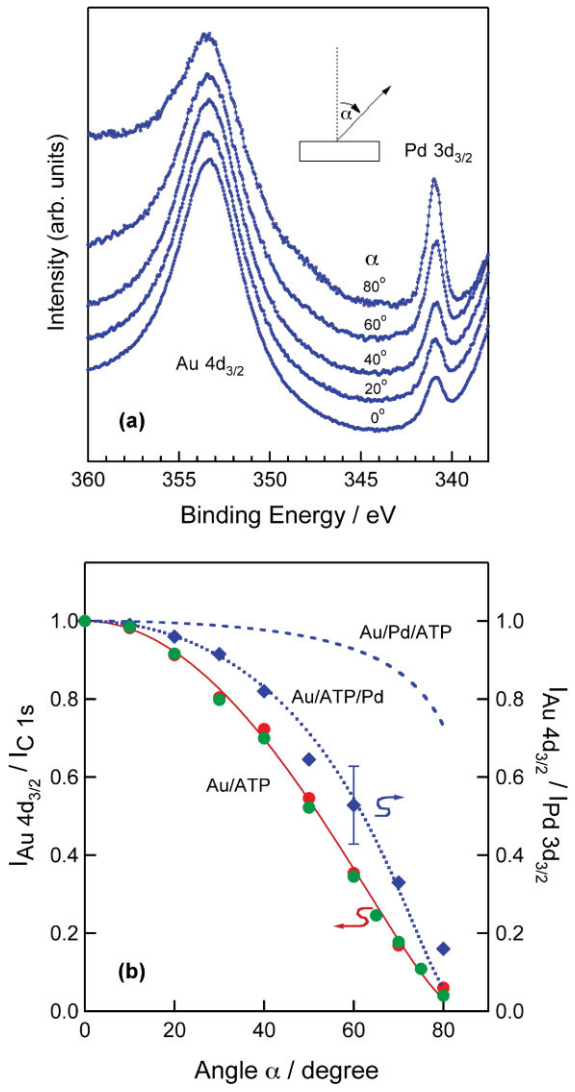

Figure 3. Angle-resolved core-level spectra covering the binding energy range of the Au $4d_{3/2}$ as well as Pd $3d_{3/2}$ core lines (a) together with ratios of the Au $4d_{3/2}$ and C-1 s line intensities (left scale) as well as the Au $4d_{3/2}$ and Pd $3d_{3/2}$ line intensities (right scale) as a function of the photoelectron detection angle (b). Experimental data are represented by full symbols, theoretical values assuming different layer sequences are shown as lines.

from buried layers within the molecular device should be significantly enhanced, which enables a critical comparison with models of both the Pd layer residing on top of the 4-ATP SAM or underneath the SAM, respectively.

The experimental results are summarized in Figure 3b where the ratios of the integrated intensities that originate from the gold substrate and either the SAM (left scale, red dots) or the Pd layer (right scale, diamonds) are plotted as a function of α, both normalized to the respective values found for emission in the normal direction. In order to test whether or not a standard formulae for angle resolved photoemission, assuming a simple layer model, can be applied, a reference sample consisting of only the SAM deposited on Au(111) (i.e., without Pd deposition) has been measured under identical conditions, which yielded the green dots shown in Figure 3b. Obviously, with or without additional Pd atoms, identical angular dependences of the carbon signals with respect to the gold substrate are observed. This provides confidence that a simple layer model assuming a continuous organic layer with identical thicknesses in both cases is appropriate to analyze the structural setup of the molecular junction in more detail.

The measured intensity ratios can be compared with predictions obtained by assuming that each overlayer attenuates the intensity of the photoelectrons escaping from the underlying layers. As a first step, using a mean free path value of 3.4 nm for Au 4d (C 1s) photoelectrons passing through a hydrocarbon film,[17] the thickness of the 4-ATP layer can be derived from Figure 3b by fitting a simple bilayer model (SAM on Au) to the experimental data (solid line). In this way, a layer thickness of about 1.8 nm can be extracted, a value that points to a molecular double layer rather than to a monolayer. As a second step, using a mean free path valve of 1.7 nm for Au 4d (C 1s) photoelectrons travelling through a metallic layer,[18] and taking into account the deposition of 60% of a Pd monolayer as shown before, the dependence of the corresponding intensity ratios on α for the two possible layer sequences (Au/SAM/Pd, Au/Pd/SAM) can be calculated. The resulting data have been added to Figure 3b where, within the error bars, excellent agreement is found between the experimental and the calculated values for the sequence Au/SAM/Pd (dotted line). In clear contrast, the results predicted for the Pd atoms residing underneath the organic layer (dashed curve) significantly deviate from the measured values. Thus, angle-resolved XPS unequivocally proves the successful electrochemical metallization of the molecular bilayer, which is in contrast to other electrochemical methods where the metallization of thiol-covered Au can also result in the intercalation of the metal between the SAM and its Au support.[19]

In order to elucidate the electronic properties of the molecular junction in more detail using DFT calculations, a $(\sqrt{3} \times \sqrt{3})$ R30° structure of the adsorbed organic layer, which leads to a 4-ATP coverage of 1/3 per layer, is taken into account, as found earlier.[20] As for the second 4-ATP layer, we used motifs of the 4-ATP bulk structure as an input for our structure optimization: the sulfur atoms of the second molecular layer are bound to three lower-lying 4-ATP molecules by S···H hydrogen bonds. On top of the 4-ATP double layer, a Pd(111) layer is placed, reflecting the highest packing density in a two-dimensional arrangement of atoms. According to our calculations, the amino group of the 4-ATP is only weakly interacting with the Pd layer. However, it is energetically more favourable by about 1 eV if the amino group becomes dehydrogenated with the hydrogen atoms being attached to the top of the Pd layer. The bare nitrogen atom then strongly binds to three Pd atoms within a three-fold coordination. The resulting Au(111)/SAM/Pd(111) structure is illustrated in Figure 4. Interestingly enough, the energy gain upon the dehydrogenation of the amino group and the formation of the Pd–N bonds is larger by 0.2 eV for the 4-ATP double layer compared with a 4-ATP single layer, since the second 4-ATP layer can more easily rearrange upon dehydrogenation. This provides an additional driving force for the stabilization of the 4-ATP double layer system induced by the metal over layer.

The structural model as shown in Figure 4 finally allows access to the local density of states (LDOS) of the Pd overlayer, which is

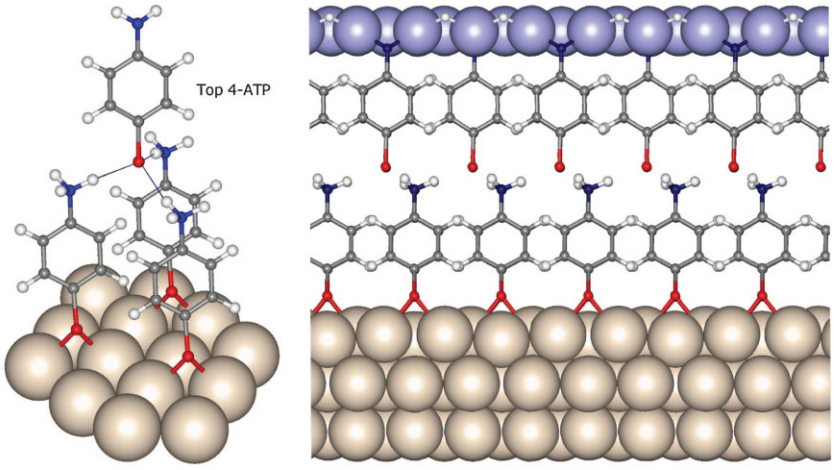

Figure 4. Illustration of the bonding within the 4-ATP double layer structure (left side) and side view of the computed DFT geometry of the Au(111)/4-ATP–4-ATP/Pd structure with the amino group of 4-ATP being dehydrogenated and the corresponding hydrogen atoms moved on top of the Pd layer (right side).

shown in Figure 5 (curve b) together with a simulated spectrum that takes into account the finite energy resolution of the experimental setup as well as the generally observed broadening of spectroscopic features because of the finite lifetime of the photoionized states (curve c). For comparison, DFT results obtained for a (hypothetical) non-interacting, free Pd layer have been added (curve a), together with UPS results extracted from the valence band spectrum of the Au/SAM/Pd junction after subtracting the corresponding spectrum acquired on a Au/SAM sample, the difference spectrum thus representing the electronic properties of the metal overlayer (curve d). In the latter case, two prominent spectroscopic features can be recognized at binding energies of 1.8 and 3.0 eV, which can be reproduced reasonably well by the DFT calculations performed for the interacting Pd layer, but certainly not by the results representing the free Pd layer. As can be seen from Figure 5, the strong Pd–N interaction leads to a significant downshift of the density of states maximum found at 0.2 eV (free layer) to about 1.6 eV (interacting layer), in good agreement, with the experiment. Note, that this downshift is not caused by the interaction of the two additional hydrogen atoms with Pd. Atomic hydrogen adsorption hardly changes the LDOS of Pd, as our and previous[21] calculations confirm. It has to be pointed out that the relative intensities of the synthetic valence band spectrum are not well reproduced, which might be attributable to matrix element effects present in the photoemission process. On the other hand, the molecular junctions were prepared in solution, whereas no electrolyte is considered in our calculations. Water itself, which is only weakly bound to Pd,[22] hardly changes the electronic structure of the metal overlayer, as was carefully checked with DFT calculations. However, there might still be a small contribution of additional, stronger bound, adsorbates like sulfur- or nitrogen-containing molecules present in the solution whose adsorption would influence the electronic structure of the Pd layer, as calculations with NH_2CH_3, $SHCH_3$, or SCH_3 adsorbed on the Pd layer indicate.

According to our calculations, the strong interaction between the metal overlayer and the supporting 4-ATP molecules results in a drastically reduced DOS at the Fermi energy E_F by nearly one order of magnitude (factor 8), as compared with a non-interacting overlayer (compare curves a and b, Figure 5). A similar behaviour, though less pronounced, has been observed recently for a Pd overlayer on a 4-mercaptopyridine SAM (reduction by a factor of 4).[13] Since the contact conductance in a molecular junction critically depends on the availability of conduction states at E_F in the metal electrodes,[23] the reduction of the DOS at E_F observed here should result in a significantly increased contact resistance, as compared with the undisturbed electrode material. Since molecules need to be attached to metal electrodes by strong chemical bonds (to guarantee stable conditions during operation) in future nanoelectronic devices this phenomenon, on one hand, represents a severe drawback for molecular electronics. On the other hand, it offers the opportunity to design sensors for molecular recognition in

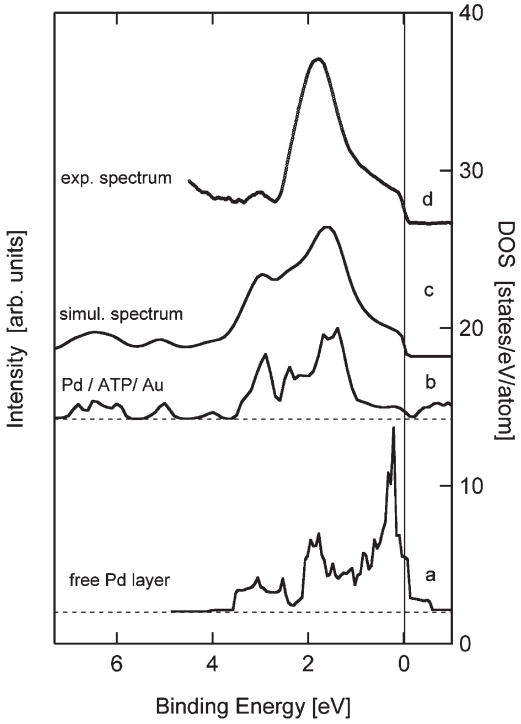

Figure 5. Theoretical (right scale) and experimental (left scale) DOS of a Pd overlayer on top of 4-ATP–4-ATP/Au(111): DFT results obtained for a free, non-interacting Pd(111) layer (curve a); calculated results for a Pd(111) layer on top of 4-ATP–4-ATP/Au(111) summed over the three inequivalent Pd sites per $(\sqrt{3} \times \sqrt{3})$ R30° surface unit cell (curve b); for better comparison with experimental results, the calculated DOS has been convoluted with a Lorentian and a Gaussian to account for the finite lifetime of the photoionized state and the energy resolution of the hemispherical analyzer, respectively (curve c); experimental DOS of a Pd overlayer as determined by UPS, extracted from the valence band spectrum of the Au/SAM/Pd junction after subtracting the corresponding spectrum acquired on a Au/SAM sample (curve d).

appropriate solutions by monitoring the increase in (contact) resistance during the bridging of a tunnelling gap between two metal electrodes by specific molecules, as has been demonstrated recently.[6]

In conclusion, the interaction between a 4-ATP self-assembled monolayer metallized by a Pd overlayer using a recently developed electrochemical approach was studied and interpreted by a combination of electron spectroscopic methods and simulations based on density functional theory. Evidence is found for the formation of a bilayer of molecules forming the SAM. Most important, strong chemical interactions between the metal atoms and the organic molecules are observed, which result in a drastically reduced density of states at the Fermi level for the metal overlayer, a quantity of utmost importance for the charge transport across the metal–molecule interface. These observations provide insight into a recently proposed method for the detection of small molecules in solution by monitoring the tunnelling resistance between two metal electrodes upon molecular adsorption.

Experimental

Sample Preparation: The preparation procedure for the metallization of the 4-ATP SAM is the same as the one described previously for 4-mercaptopyridine [7,9,10]. In essence it consists of three steps: a) The freshly annealed Au(111) electrode, a single-crystal disc of 8 mm diameter and 2 mm thickness (MaTeck, Jülich, Germany), was immersed for different lengths of time (1–15 min) in a 0.1×10^{-3} M solution of 4-ATP in aqueous 0.1 M H_2SO_4 without potential control. The solution was de-aerated to prevent thiol oxidation. b) After thoroughly rinsing the thiol-modified gold electrode with water, the sample was immersedagain without potential control and for different lengths of timein 0.1×10^{-3} M $PdSO_4$/0.1 M H_2SO_4 to allow Pd ion adsorption/complexation with the amino group of the SAM. c) After rinsing again with water, the immersed electrode was then transferred to the electrochemical cell, which contained neat 0.1 M H_2SO_4. The electrode was contacted with the electrolyte at +0.6 V vs. SCE to prevent unintentional reduction of the adsorbed Pd^{II}, and the potential scan was started in the negative direction for electroreduction of the Pd ions.
All solutions were prepared with ultra-pure water (Satorius, Germany, total organic carbon <3 ppb, 18.2 MΩcm) and supra-pure H_2SO_4 (Merck). 4-ATP (Aldrich, 90%) was used as received. All potentials are quoted vs. SCE, although for the STM experiments a Pt wire served as a pseudo-reference electrode ($E_{Pt} = +0.55 \pm 0.05$ V vs. SCE). For cyclic voltammetry standard electrochemical equipment was used.

Photoelectron Spectroscopy: Photoemission spectra were acquired on a Fisons ESCALAB 210 electron spectrometer to allow analysis of the chemical state of the samples and their layer sequence by XPS using monochromatized X-rays (1486.6 eV). The electronic structure of the Pd overlayer was determined using UPS performed with non-polarized He-II radiation (40.8 eV) as provided by a gas discharge lamp. In both cases, the angular acceptance of the energy analyzer was set to its maximum value (±12°) in order to avoid photoelectron diffraction effects as a result of the single crystalline substrate and to average over the surface Brillouin zone of the metal overlayer thus allowing interpretation of the corresponding UPS spectra in terms of electronic densities of states. Radiation damage to the SAM could be avoided by the small spot size of the two photon beams (<1 mm) allowing a certain sample position to be probed for times of about 1 h, followed by moving to a new position. During these probing times, no measurable changes of the corresponding core-level or valence-band intensities, or changes in their line shapes, were detected.

Theoretical Approach: In order to elucidate the geometric and electronic structure of the metallized 4-ATP SAM, periodic DFT calculations were carried out using the DFT code VASP [24] with the PBE functional [25] to describe the exchange-correlation effects. The core electrons were treated by the projected augmented wave method [26]. The electronic wave functions were expanded in a plane-wave basis set with an energy cut-off of 400 eV. The Au(111) substrate was described by a slab with a thickness of three layers.

Acknowledgements

Financial support by the Odysseus program of the Flemish Government, the Deutsche Forschungsgemeinschaft (DFG) within SFB 569, the Swiss National Science Foundation (NF), and the Swiss National Center of Competence in Research (NCCR) 'Nanoscale Science' is gratefully acknowledged. The authors also thank F. Eberle (Univ. of Ulm) for technical support and P. Ziemann (Univ. of Ulm) for discussions.

Received: June 16, 2008
Published online:

[1] A. Aviram, M. Ratner, *Chem. Phys. Lett.* **1974**, *29*, 277.
[2] M. A. Reed, C. Zhou, C. J. Muller, T. P. Burgin, J. M. Tour, *Science* **1997**, *278*, 252.
[3] C. Joachim, J. K. Gimzewski, A. Aviram, *Nature* **2000**, *408*, 541.
[4] J. Reichert, R. Ochs, D. Beckmann, H. B. Weber, M. Mayor, H. v. Löhneysen, *Phys. Rev. Lett.* **2002**, *88*, 176 804.
[5] S. M. Lindsay, M. A. Ratner, *Adv. Mater.* **2007**, *19*, 23.
[6] X. Dong, Y. Xia, G. Zhu, B. Zhang, *Nanotechnology* **2007**, *18*, 395502.
[7] T. Baunach, V. Ivanova, D. M. Kolb, H.-G. Boyen, P. Ziemann, M. Büttner, P. Oelhafen, *Adv. Mater.* **2004**, *16*, 2024.
[8] V. Ivanova, T. Baunach, D. M. Kolb, *Electrochim. Acta* **2005**, *50*, 4283.
[9] M. Manolova, V. Ivanova, D. M. Kolb, H.-G. Boyen, P. Ziemann, M. Büttner, A. Romanyuk, P. Oelhafen, *Surf. Sci.* **2005**, *590*, 146.
[10] M. Manolova, M. Kayser, D. M. Kolb, H.-G. Boyen, P. Ziemann, D. Mayer, A. Wirth, *Electrochim. Acta* **2007**, *52*, 2740.
[11] V. Batz, M. A. Schneeweiss, D. Kramer, H. Hagenström, D. M. Kolb, D. Mandler, *J. Electroanal. Chem.* **2000**, *491*, 55.
[12] M. Manolova, *Structure of and metal deposition on thiol covered Au(111) surfaces*, Ph.D. Thesis, Universität Ulm **2006**.
[13] H.-G. Boyen, P. Ziemann, U. Wiedwald, V. Ivanova, D. M. Kolb, S. Sakong, A. Gross, A. Romanyuk, M. Büttner, P. Oelhafen, *Nat. Mater.* **2006**, *5*, 394.
[14] O. Shekhah, C. Busse, A. Bashir, F. Turcu, X. Yin, P. Cyganik, A. Birkner, W. Schuhmann, C. Wöll, *Phys. Chem. Chem. Phys.* **2006**, *8*, 3375.
[15] A. Groß, *J. Comput. Theor. Nanosci* **2008**, *5*, 894.
[16] H. Kind, A. M. Bittner, O. Cavalleri, K. Kern, T. Greber, *J. Phys. Chem. B* **1998**, *102*, 7582.
[17] P. E. Laibinis, C. D. Bain, G. M. Whitesides, *J. Phys. Chem. B* **1991**, *95*, 1717.
[18] D Briggs,, M. P. Seah, Eds., *Practical Surface Analysis*, *Vol. 1*, Wiley, Chichester **1996**.
[19] C. Silien, M. Buck, *J. Phys. Chem. C* **2008**, *112*, 3881.
[20] Y.-T. Kim, R. L. McCarley, A. J. Bard, *J. Phys. Chem. B* **1992**, *96*, 7416.
[21] M. Lischka, A. Groß, *Phys. Rev. B* **2002**, *65*, 0 757 420.
[22] A. Roudgar, A. Groß, *Chem. Phys. Lett.* **2005**, *409*, 157.
[23] S. Stojkovic, C. Joachim, L. Grill, F. Moresco, *Chem. Phys. Lett.* **2005**, *408*, 134.
[24] G. Kresse, J. Furthmüller, *Phys. Rev. B* **1996**, *54*, 11 169.
[25] J. P. Perdew, K. Burke, M. Ernzerhof, *Phys. Rev. Lett.* **1996**, *77*, 3865.
[26] P. E. Blöchl, *Phys. Rev. B* **1994**, *50*, 17 953.